Chapter 14
Steam Turbines

Chapter 7 dealt with the class of rotating machines called "turbomachines". These devices are usually driven by some form of prime mover such as an electric motor or steam turbine. As well as driving pumps and compressors, and as the most widely used form of marine propulsion, the most common usage of large steam turbines is driving electric generators in central power stations.

An early steam turbine was demonstrated in 1896 by C. H. Parsons in a small but fast torpedo boat, the "Turbinia". The steam turbine's advantages of high speed, high power, compact dimensions and good reliability led to its widespread adoption for marine propulsion, and it quickly replaced the heavy and slow reciprocating engines of the day.

Early turbines had a single row of blades. Parsons' turbine used several rows of reaction blading to distribute the pressure drop over several stages. This was followed in 1896 by the invention by Curtis of the multi-row velocity-compound turbine. Modern turbines use a combination of stage types but still employ the physical principles of these pioneering designs.

14.1 Steam Expansion Through the Turbine

A single turbine expansion stage consists of

(a) A fixed convergent/divergent Laval nozzle which converts potential energy represented by pressure to kinetic energy represented by velocity.
(b) A rotating set of blades which convert momentum (kinetic energy) of the steam flow to mechanical work

Two types of turbine stage are used, impulse and reaction. In the impulse stage most pressure conversion takes place in the stationary nozzles with little change in pressure in the moving blades. In the reaction stage most pressure conversion takes place in the rotating blades. The following analysis does not distinguish between

P. O'Kelly, *Computer Simulation of Thermal Plant Operations*,
DOI 10.1007/978-1-4614-4256-1_14,

Fig. 14.1 A boiler feedpump turbine, open for inspection (courtesy of Millmerran Operating Company, Australia)

the two types as the overall effects of each are sufficiently similar. Most turbines use one impulse stage as the first HP stage for speed and power control with the others being reaction stages. It is usual to operate the impulse stage in the choked condition for speed control; otherwise, stable speed control, with the turbogenerator unsynchronised, is difficult.

Figure 14.1 shows a turbine used to drive a boiler feed pump. As the turbine is operated with variable speed, the first stage is an impulse row followed by (in this case) four reaction rows. The characteristic shapes of the individual blades—impulse or reaction—are clearly visible in the picture.

Following Traupel [61], the mass flow through a turbine expansion stage is calculated from the general nozzle equation

$$\dot{m}^2 = \left(C_T \sum_i a_i \varepsilon_i \right)^2 \frac{\gamma}{\gamma + 1} \frac{p_1}{v_1} \left[1 - \left(\frac{p_1}{p_2} \right)^{\frac{\gamma+1}{\gamma}} \right], \tag{14.1}$$

where γ is the adiabatic index defined by the state equation for steam

$$pv^{\gamma} = \texttt{constant}.$$

The constant C_T is the stage flow coefficient and is substantially independent of operating conditions. The term $\sum_i a_i \varepsilon_i$ is the summation of the individual admission areas where a_i is the full area of the i-th admission stage and ε_i is the admission fraction of the i-th stage. This is relevant only to the first (control) stage and only to turbines provided with partial arc admission control. The subscript "1" denotes the upstream variable, "2" the downstream variable.

This equation can be written in terms of the stage design conditions, denoted by the subscript "0", assuming that C_T is constant for all operating conditions and that the stage operates with full arc admission under design conditions.

$$\left(\frac{\dot{m}}{\dot{m}_0}\right)^2 = \left(\frac{p_1 v_{10}}{p_{10} v_1}\right)\left(\frac{1-(p_2/p_1)^{\frac{\gamma+1}{\gamma}}}{1-(p_{20}/p_{10})^{\frac{\gamma+1}{\gamma}}}\right)$$

$$= \left(\frac{p_1}{p_{10}}\right)^2\left(\frac{p_{10} v_{10}}{p_1 v_1}\right)\left(\frac{1-(p_2/p_1)^{\frac{\gamma+1}{\gamma}}}{1-(p_{20}/p_{10})^{\frac{\gamma+1}{\gamma}}}\right)$$

$$= \left(\frac{p_1}{p_{10}}\right)^2\left(\frac{\mathcal{T}_{10}}{\mathcal{T}_1}\right)\left(\frac{1-(p_2/p_1)^{\frac{\gamma+1}{\gamma}}}{1-(p_{20}/p_{10})^{\frac{\gamma+1}{\gamma}}}\right), \tag{14.2}$$

where $\mathcal{T}_{10}$ and $\mathcal{T}_1$ are expressed in degrees K.

This equation is valid only for an infinite series of turbine stages. For a finite number of stages, and particularly for a single stage, the pressure ratio function must be modified to reflect the existence of a critical ratio beyond which the flow velocity reaches sonic velocity, and the mass flow rate becomes independent of downstream conditions (the choked flow condition mentioned earlier). An appropriate function valid for all pressure ratios ≤ 1 is, with $\Pi = p_2/p_1$,

$$e = \left[1-\left(\frac{\Pi-\Pi_{cr}}{1-\Pi_{cr}}\right)^{\frac{\gamma+1}{\gamma}}\right]^{1/2}$$

$$e = 1 \quad \text{for} \quad \Pi \leq \Pi_{cr}.$$

We may then write

$$\frac{\dot{m}}{\dot{m}_0} = \left(\frac{p_1}{p_{10}}\right)\sqrt{\frac{\mathcal{T}_{10}}{\mathcal{T}_1}}\left(\frac{e}{e_0}\right). \tag{14.3}$$

Since e is a function of the ratio of downstream to upstream pressures, this equation contains all the information necessary for the computation of the complete condition line on the basis of conservation of mass in each stage.

The normalised flow ratios calculated using Eqs. 14.2 and 14.3 are shown in Fig. 14.2 for a range of p_2 from zero to p_1. The turbine stage parameters are assumed to have their nominal or rated values.

As shown in Fig. 4.1, γ can be expected to lie in the range 1.25–1.3 for most operating conditions of interest. The ratio $(\gamma+1)/\gamma$ is then sufficiently close to 2 to allow the writing of Eq. 14.3 as

$$e^2 = 1-\left(\frac{\Pi-\Pi_{cr}}{1-\Pi_{cr}}\right)^2. \tag{14.4}$$

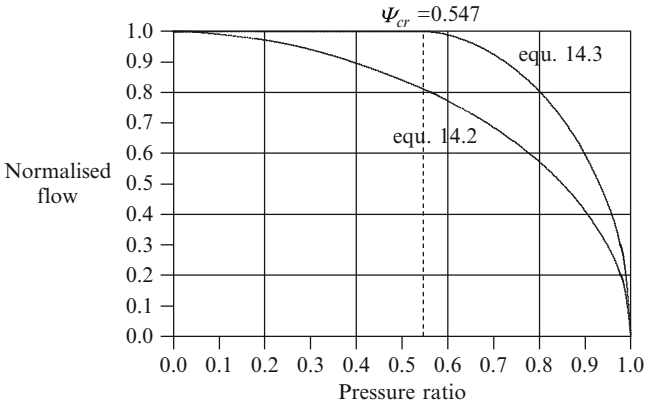

Fig. 14.2 Steam turbine flow characteristics

With this approximation, and noting that $p_2 = p_1 - \Delta p$, where Δp is the pressure differential across the stage, Eq. 14.4 may be resolved to

$$e^2 = \left(\frac{2}{1-\Pi_{cr}}\right)\frac{\Delta p}{p_1} - \left(\frac{2}{(1-\Pi_{cr})^2}\right)\left(\frac{\Delta p}{p_1}\right)^2$$

for $\Pi \geq \Pi_{cr}$. Since $\Delta p \ll p_1$, this may be written without the quadratic term as

$$e^2 = \left(\frac{2}{1-\Pi_{cr}}\right)\frac{\Delta p}{p_1} \tag{14.5}$$

allowing Eq. 14.3 to be written as

$$\frac{\dot{m}}{\dot{m}_0} = K_t\left(\frac{p_{in}}{p_{in0}}\right)\sqrt{\frac{\mathcal{T}_{in0}}{\mathcal{T}_{in}}}\left(\frac{1}{e_0}\right)\sqrt{\frac{\Delta p}{p}}, \tag{14.6}$$

where p_{in} and T_{in} are the steam pressure and temperature before the first blade row and as above, the subscript "0" denotes the rated value. Turbines are usually designed to operate with approximately equal pressure ratios across all stages, and the flow function e_0 can be evaluated using the design ratio Π_0.

$$e_0 = \left[1 - \left(\frac{\Pi_0 - \Pi_{cr}}{1-\Pi_{cr}}\right)^{\frac{\gamma+1}{\gamma}}\right]^{1/2}.$$

Ideally,

$$K_t = \sqrt{2/(1-\Pi_{cr})} = 2.1012 \tag{14.7}$$

but the approximations involved in the reduction of Eq. 14.3 to Eq. 14.6 introduce some error. The constant can be adjusted if necessary to match the known characteristic of a reference turbine.

If the dynamics of steam flow through the turbine are ignored, the following algebraic procedure may be used to calculate steam conditions after each blade row.

Inlet flow:

$$\dot{m}_{in} = \dot{m}_0 \left(\frac{p_{in}}{p_{in0}}\right) \sqrt{\left(\frac{\mathcal{T}_{in0}}{\mathcal{T}_{in}}\right)}. \tag{14.8}$$

For the downstream rows:

$$\begin{aligned} p_j &= \Pi_0 p_{j-1}, \\ \dot{m}_j &= \dot{m}_{j-1} - \dot{m}_{bl,j} - \dot{m}_{dr} \pm \dot{m}_{gss}, \\ T_j &= (T_{j-1} + 273) \left(\frac{p_j}{p_{j-1}}\right)^{\frac{\gamma-1}{\gamma}} - 273, \\ v_j &= f(p_j, T_j), \end{aligned}$$

where $\dot{m}_{bl}$, $\dot{m}_{dr}$ and $\dot{m}_{gss}$ are bled steam, drain and gland sealing flows.

The assumption of equal pressure ratios for all blade rows is satisfactory if no extraction flows are taken or if extraction flows are much less than the main steam flow, as is usually the case. A general solution allowing variable pressure ratios to accommodate extraction flows, drain and gland sealing flows can be developed for the complete cylinder from a statement of conservation of mass for each blade row. Then, with the introduction of a blade row "capacitance" C_j, we can write for the j-th row,

$$C_j \frac{\mathrm{d}p_j}{\mathrm{d}t} = \dot{m}_{j-1} - \dot{m}_j - \dot{m}_{bl,j} - \dot{m}_{dr} \pm \dot{m}_{gss}. \tag{14.9}$$

The mass flow $\dot{m}_j$ is obtained from Eq. 14.6. Then, for the j-th blade row,

$$\begin{aligned} \dot{m}_j &= \dot{m}_0 K_t \left(\frac{p_{in}}{p_{in0}}\right) \sqrt{\frac{\mathcal{T}_{in0}}{\mathcal{T}_{in}}} \left(\frac{1}{e_0}\right) \sqrt{\frac{\Delta p_j}{p_j}} \\ &= \mathcal{A}_t \sqrt{\frac{\Delta p_j}{p_j}} \\ &= \mathcal{A}_t \frac{1}{\sqrt{(p_j \Delta p_j)}} (p_{j-1} - p_j), \end{aligned} \tag{14.10}$$

where

$$\mathcal{A}_t = \dot{m}_0 K_t \left(\frac{p_{in}}{p_{in0}}\right) \sqrt{\frac{\mathcal{T}_{in0}}{\mathcal{T}_{in}}} \left(\frac{1}{e_0}\right)$$

whose component terms are known from design data and the current turbine inlet conditions. The linearisation

$$\sqrt{\frac{\Delta p_j}{p_j}} = \frac{\Delta p_j}{\sqrt{(p_j \Delta p_j)}}$$

assumes the denominator terms of the right-hand side are known from the preceding time step.

Equation 14.10 may be expanded for all blade rows and inlet and outlet boundary conditions. The resulting tridiagonal equation yields the profile of pressures through the turbine for the given boundary conditions and extraction, drain and gland sealing flows.

Conditions at the turbine inlet are defined by the nozzle box pressure p_{in}, steam enthalpy h_{in} and temperature T_{in} together with the resulting inlet flow $\dot{m}_{in}$ calculated from Eq. 14.8. The pressure after the last row is defined by conditions external to the turbine exhaust. Where the turbine exhausts to a steam line, as in a back-pressure industrial turbine drive or a turbogenerator exhausting to an air-cooled condenser, the pressure drop in the exhaust pipe or duct must be included in the calculation of the turbine exhaust pressure.

The following table presents design data for a large steam turbine used in a supercritical generating unit. The quoted pressure ratio assumes the same pressure ratio for all blade rows in the cylinder.

Cylinder	Rated flow kg/s	Inlet pressure bar	Inlet temp deg C	Exhaust pressure bar	Exhaust temp deg C	Blade rows	Pressure ratio
HP	354	242.2	566	52.62	329	27	0.945
IP	302	47.35	593	5.783	283	17	0.884
LP	259	5.782	283	0.184	58	7	0.73

The expansion line calculation can produce steam conditions at each blade row, for example, for each of the 27 HP cylinder rows. For most simulation purposes this detail is not required and several rows can be grouped to give a lesser number of equivalent rows. If the number of grouped rows were selected to yield a pressure ratio of 0.85–0.87, the 27 rows of the tabulated HP cylinder can be reduced to eight rows between inlet and the first bleed point and three rows to the exhaust. The design pressure ratio is selected to match the design data of the reference turbine. The following table sets out the calculated pressures and temperatures at the bleed and exhaust rows for four different loads, calculated using the expanded version of Eq. 14.10, together with the actual design figures.

% CMR	100	75	50	25
Design inlet pressure kPa	24,220	18,950	12,510	11,220
Design inlet temperature °C	566	566	544	515
Design inlet flow kg/s	354	254	170	91
Calculated inlet flow kg/s	350	261	175	91
Calculated first-stage pressure kPa	24,220	18,950	12,510	6,358
Design bleed point pressure kPa	7,655	5,603	3,760	1,913
Calculated bleed point pressure kPa	7,652	5,715	3,865	2,002
Design bleed point temperature °C	379	380	369	334
Calculated bleed point temperature °C	382	394	377	341
Design exhaust pressure kPa	5,262	3,878	2,613	1,354
Calculated exhaust pressure kPa	5,262	3,888	2,646	1,354
Design exhaust temperature °C	329	332	323	293
Calculated exhaust temperature °C	345	341	327	297

The inlet pressure and temperature values quoted are those before the turbine throttle valves. The table is based on sliding pressure operation down to around 50% CMR, with fully open throttle valves. Below 50% turbine power is controlled by the throttle valves while holding steam pressure constant. For the calculation of turbine conditions at 25% CMR for this table, the throttle valves were closed to match the known design flow.

14.2 Developed Work in the Energy Balance

An additional term must be added to the energy balance equation for a turbine stage to provide for the mechanical work done by the turbine stage which does not appear as heat transferred. This is denoted W_j [kJ/s] being the mechanical work done by steam expansion in the j-th expansion stage.

The mechanical work done is computed as the product of the steam flow through the stage and the real specific enthalpy drop across the stage.

$$W_j = \dot{m}_j \Delta h_j . \tag{14.11}$$

The total work done by all stages is the sum of the individual stage works.

$$W_\Sigma = \sum_j W_j . \tag{14.12}$$

It can be shown that, for adiabatic expansion from p_j to p_{j+1}, the ideal enthalpy difference across the stage is

$$\Delta h_{s,j} = \frac{\gamma}{\gamma - 1} p_j v_j \left[1 - \left(\frac{p_{j+1}}{p_j} \right)^{\frac{\gamma-1}{\gamma}} \right]. \tag{14.13}$$

The real specific enthalpy differential is given as $\Delta h_s \eta_p$, where η_p is the stage expansion efficiency.

Expansion in a turbine stage should be treated as a polytropic process as the stage incurs irreversible losses. The adiabatic index in Eq. 14.13 is replaced by the polytropic index, defined in Sect. 4.2 as

$$\frac{n}{n-1} = \frac{1}{\eta_p} \frac{\gamma}{\gamma - 1} \tag{14.14}$$

as we are considering expansion. After making this substitution Eq. 14.13 becomes, now for the real enthalpy differential across the stage,

$$\Delta \hat{h}_{s,j} = \frac{n}{n-1} p_j v_j \left[1 - \left(\frac{p_{j+1}}{p_j} \right)^{\frac{n-1}{n}} \right]. \tag{14.15}$$

14.3 Moisture Production Within the Turbine Stage

Moisture will be formed within the turbine under the following conditions:

- During start-up warming, steam will condense on cold parts; the condensate is removed through casing drains. Condensate mass flow rates are computed for all operating conditions (i.e. not just start-up) on the basis of heat transfer from the steam to the condensing surfaces. Under normal loaded operation, condensation is unlikely as the condensing surfaces will be close to steam temperature.
- During normal operation (well-developed steam flow through the blading) a water phase develops wherever the steam enthalpy reduces below the local saturation enthalpy. The mass flow rate is defined by the steam wetness factor and the total steam flow rate. The water phase is removed via the moisture separator for each stage and the total moisture passed to the drains cooler.

Modern steam turbines can achieve HP and IP thermal efficiencies of around 93–96%. LP turbines achieve lower values, but overall efficiencies of multi-cylinder sets will exceed 90% at full load.

The moisture flow rate for the j-th stage is calculated from

$$\begin{aligned} x &= \frac{h_s - h'}{h'' - h'}, \\ \dot{m}_w &= (1 - x)\dot{m}_j, \end{aligned} \tag{14.16}$$

where x is the steam mass fraction, h_s is the local steam enthalpy, h', h'' are the local saturation enthalpies, $\dot{m}_j$ is the steam flow into the j-th stage and $\dot{m}_w$ is the moisture flow from the stage.

14.4 Low Flow Operation

Steam turbines are optimised for full- or near-full-load operation. At low flows (typically $< 25\%$) and particularly during start-up, steam flows are very low and the flow patterns through blades can depart from the ideal flow regimes. This leads to reduced efficiencies in all cylinders but because of its long blades and particularly those of the last row, the LP turbine is particularly vulnerable to water droplet erosion by wet steam, heating due to friction losses and blade vibration due to turbulent and vortex flows between the blades. Instances of blade failure have been attributed to these flow pattern disturbances [62]. Specifically the last row of the LP turbine, the exhaust area of which strongly influences the power capability of the turbine, must be protected from these effects and so-called turbine exhaust hood sprays are provided to keep LP turbine exhaust temperatures down during start-up and periods of low steam flow.

14.5 Gland Sealing Steam Flows

The casing enclosing a rotating turbomachine (turbine or compressor) is supported at each end by a pedestal which also carries the shaft bearing and the shaft gland seal. Gland seals are intended both to prevent the entry of air into a casing through the gap between shaft and casing and to minimise loss of the working medium from the casing through the gap. In the absence of a seal, with subatmospheric pressure in the casing, air can enter the casing along the shaft. Similarly, with a high pressure in the casing, the working medium can flow outwards along the shaft. The entry of air is prevented by creating a positive ($>$ atmospheric) pressure between the outside air and the casing. This is established by introducing steam[1] at an intermediate point along the seal and by creating a low admittance flow path to limit the flow of the sealing medium along the shaft. The same sealing arrangement minimises loss from the casing via the same low admittance flow path.

The most common form of gland seal is the labyrinth seal. The general arrangement is shown schematically by the following (Fig. 14.3).

[1] Water or oil are used in other applications.

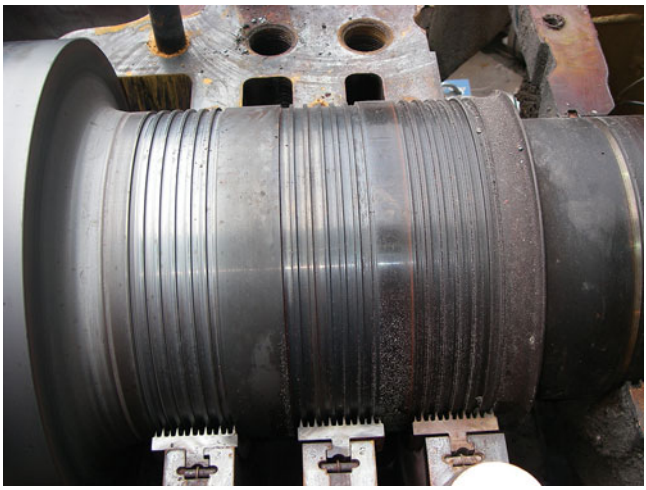

Fig. 14.3 Turbine shaft gland seals (courtesy of Millmerran Operating Company, Australia)

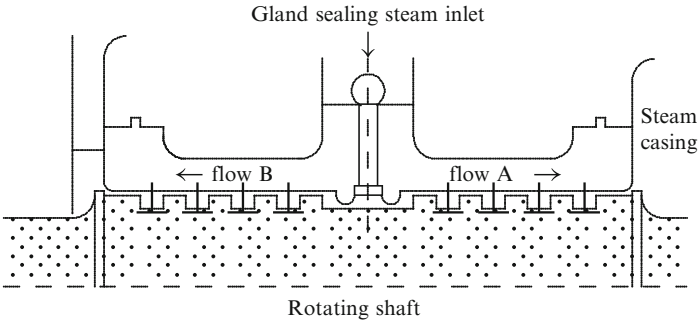

The seal consists of two circumferential rows of short, interlocking, narrowly spaced, parallel baffles arranged along the axis of the shaft. One row, mounted on the shaft, protrudes a few millimetres from the surface and meshes with a matching row inserted into the stationary casing. The complete arrangement creates a long, small cross-section path and presents high resistance to flow. We will consider the operation of a steam turbine gland seal but the principle applies to any sealing medium. Supplied from an external source to a point roughly central in the labyrinth, steam will flow both inwards into the turbine casing (flow A) and outwards towards a collection header or atmosphere (flow B). In small turbines this flow will be either collected and returned to the system or vented. In large turbines it will always be collected and returned to the system. As pressure is developed inside the turbine casing the sealing steam flow A will reverse when the casing pressure exceeds the pressure at the gland seal inlet point. A small but continuous flow of steam is lost from the turbine through the seal during normal operation.

Since the minimum labyrinth clearance c_l is much less than the shaft diameter d_{sh}, the minimum flow cross-sectional area a_{gs} is approximately $\pi\, d_{sh}\, c_l$. The flow through the seal can be calculated simply as

$$\dot{m} = a_{gs} \sqrt{\frac{p_1^2 - p_2^2}{l\ p_1 v_1}},$$

where l is the steam flow path length. Given that all stages of the seal are identical, we can replace the path length l by a factor $(1/k^2)\, n_{stg}$ where n_{stg} is the number of stages along the flow path. The preceding equation can then be written

$$\dot{m}^2 = k^2\, a_{gs}^2 \left(\frac{p_1^2 - p_2^2}{n_{stg}\ p_1 v_1} \right). \tag{14.17}$$

This can be reorganised into the form $\dot{m}^2 = \mathcal{A} \Delta p$, with $\Pi = p_2 / p_1$. Then,

$$\dot{m}^2 = \frac{k^2\, a_{gs}^2}{n_{stg} v_1} (1 + \Pi) \Delta p. \tag{14.18}$$

It is the nature of gland seals that the pressure ratio across them is very large, allowing the assumption that $\Pi \ll 1$. Then

$$\dot{m}^2 = \frac{k^2\, a_{gs}^2}{n_{stg} v_1} \Delta p. \tag{14.19}$$

The small clearances between the rotating and stationary sections of the seal set tight limit on the allowable longitudinal movement of the turbine shaft during those operational phases during which the turbine shaft may be expanding or contracting. These in turn set limits on the allowable rates of change of turbine shaft temperatures during both fast and slow transients.

Traupel [61] suggests that the minimum labyrinth clearance be determined according to the following rule, with the shaft diameter d_{sh} expressed in millimetres:

$$c_l = A\, \frac{d_{sh}}{1000} + 0.25 \text{ mm}$$

$$\text{with} \begin{cases} \text{A} = \text{0.6 for compressors} \\ \text{A} = \text{0.85 for turbines fabricated from ferritic steel} \\ \text{A} = \text{1.3 for turbines fabricated from austenitic steel} \end{cases}$$

The various values of A reflect the differing temperature environments in which compressors and turbines operate, with compressors being exposed to relatively small temperature variations and austenitic steel turbines exposed to the highest temperatures and largest temperature gradients, both static and dynamic.

The order of magnitude and dependence of gland flows on operating conditions are illustrated by the following numerical examples. These have been calculated for a gland seal on a high-pressure turbine casing with superheated steam at pressures of 1,000 kPa and 10,000 kPa in the casing (p_1) and at the point of connection of the gland sealing steam, a counter-pressure (p_2) of 200 kPa.

For a shaft diameter d_{sh} = 500 mm; then, using A = 1.3, the gland clearance is 0.9 mm giving a flow cross-section area of 1.4e−3 m^2. The gland steam flows from the HP turbine casing for the assumed steam conditions are tabulated.

Steam pressure	Steam temperature	Stages	Gland steam flow
1,000 kPa	300°C	5	0.039 kg/s
		10	0.028 kg/s
10,000 kPa	340°C	5	0.204 kg/s
		10	0.144 kg/s

Heat Transfer from Gland Sealing Steam

The steam flow through the glands will transfer heat to the shaft in the region of the glands. In view of the low velocity of the steam, heat transfer rates will be low and total heat will be low given the small flow rates. Heat transfer from the gland flows should be considered in view of the local shaft heating and expansion effects though low accuracy should suffice.

14.6 Heat Transfer from Steam to the Casings and Shaft

Heat transfer to the casing and shaft is used for the calculation of casing and shaft temperatures, casing and shaft thermal expansions and differential expansions, shaft and casing stresses, stress limits and shaft fatigue life estimation.

Heat is transferred by convection from the steam to the turbine blades, both moving and stationary, and to the turbine casing(s). Little heat is transferred directly to the shaft or internal casing, heat reaching these predominantly via conduction through the blading. A small quantity of heat is transferred directly to the shaft in the gland seals.

Figure 14.4 shows the arrangement of shaft, rotating and stationary blading, support structure and outer casing for a typical HP turbine cylinder.

Steam enters the turbine via the cavity ahead of the first-stage nozzles. Steam leaving the nozzles impinges on the first blade row (usually an impulse stage) and passes through successive rows of stationary and rotating blades (reaction stages) to the turbine exhaust. Steam leaving the last row of blades is directed back through the annular region (the annulus) between the outer casing and the inner structure

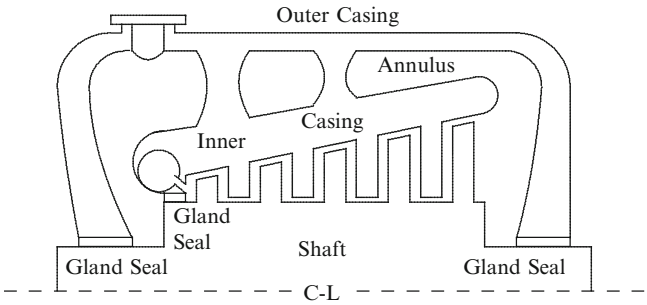

Fig. 14.4 Schematic arrangement of a return flow HP turbine cylinder

supporting the stationary blading, the inner casing. The inner casing is exposed to steam on both sides. On the blading side, the steam is at the stage temperature as given by the expansion line calculation. On the annulus side, it is at a temperature approximating the temperature of the steam leaving the stage, the turbine exhaust temperature. It is reasonable to assume this temperature since steam transits the annulus very quickly and the outer casing is well insulated. The annulus receives a small steam flow through the high-pressure shaft gland between the impulse row and the annulus. It also receives or sends a small flow through the outer casing shaft seals, depending on turbine operation.

14.6.1 Heat Transfer to the Casings

Inner Casing Annulus Side

The estimation of the heat transfer area is complicated by the geometry of the outer surface of the stationary blading support structure. This is not a smooth cylindrical surface, having a basically regular surface but including support rings connecting to the outer casing and various other departures from a regular surface. The construction details vary greatly among manufacturers. It is reasonable to define an outer diameter of an equivalent smooth cylinder which will be close to that of the identifiable inner casing cylindrical outline. Since in most HP and IP cylinder designs the stationary blading is installed along only some 2/3 of the total inner casing length, the area used per stage for the outer surface of the inner casing can be calculated as the total area divided by the number of configured stages. The total outer surface area of the inner casing is

$$A_{oc} = f_s \frac{\pi}{4} d_o^2 L_{oc}, \tag{14.20}$$

where d_0 is the equivalent outer diameter and L_{oc} is the overall length of the inner casing. f_s is a factor introduced to account for departures from the idealised surface.

Stationary Blades

The bulk of heat transferred to the inner casing travels via the stationary blading whose exposed area is much greater than the casing area exposed between the blade rows. The heat transfer area therefore approximates the blade area which for a single blade can be approximated by

$$A_{bl} = 2\, l_{bl}\, c_{bl}\, f_a, \tag{14.21}$$

where l_{bl} is the average length of blading (from root to tip) and c_{bl} is the average chord length of the blades (distance from leading to trailing edge). The factor 2 includes both sides of the blades. Because the blades have an airfoil profile, the factor f_a is applied to allow for surface curvature and might be expected to take a value in the range 1–1.2.

Heat transfer to the stationary blades can be treated on a per-blade-pair basis using the heat transfer coefficient from Eq. 8.13. The mass flow density ϕ is calculated from the turbine exhaust flow $\dot{m}_s$ as

$$\phi = \frac{\dot{m}_s}{n_{bls}} \frac{1}{A_{bls}},$$

where n_{bl} is the number of blades in the j-th row, $n_{bls} = n_{bl} - 1$ is the number of inter-blade spaces and, with δb the average blade-blade separation, $A_{bls} = l_{bl}\delta b$ is the flow area between adjacent blades. The equivalent diameter d_{eq} is calculated from

$$d_{eq} = \frac{4\, A_{bls}}{U_{fs}},$$

where $U_{fs} = 2(l_{bl} + \delta b)$.

Conduction along the blading is included by assuming that this can be represented by a conduction path per blade of length equal to 1/2 of the average blade length l_{bl}. The overall heat transfer coefficient for heat transfer from the steam to the inner casing is then given as

$$\frac{1}{\alpha_1} = \frac{1}{\alpha_0} + \frac{l_{bl}/2}{\lambda A_{x,bl}\, f_c}, \tag{14.22}$$

where $A_{x,bl}$ = (chord x thickness) is the mean blade cross-sectional area [m^2]. Again, f_c is a factor introduced to account for the non-rectangular cross-section of the blade and will take a value in the range 0.5–0.75.

Heat transferred to the inner casing at the j-th turbine stage is then

$$\dot{q}_1^j = \alpha_1^j \, a_{bl}^j \, n_{bl} (T_s^j - T_m^j), \tag{14.23}$$

where T_s^j is the local steam temperature and T_m^j is the local casing temperature.

Heat Transfer from the Inner Casing to the Annulus Steam

Heat is conducted through the inner casing and by convection to the steam in the annulus. The heat transfer coefficient on the annulus side is given by the standard Hausen correlation, Eq. 8.9, with flow and steam thermodynamic conditions defined by the turbine stage exhaust. The steam mass flow density ϕ used by this correlation is determined as

$$\phi = \dot{m}_{exh} / A_{ann},$$

where $\dot{m}_{exh}$ is the mass flow leaving the last blade row and A_{ann} is the representative annular area between the inner and outer casings. This area is of course not uniform, but uniformity is a workable assumption.

The total heat transferred to the steam in the annulus from the inner casing is the sum of the heat transferred from each inner casing cell, assuming a uniform steam temperature in the annulus. For most operational phases, this is a probably true.

$$\dot{q}_{ic} = \sum_{j=1}^{j=n_c} \dot{q}_{ic}^j, \tag{14.24}$$

where, with T_{sa} is the representative temperature of the steam within the annulus,

$$\dot{q}_{ic}^j = \alpha_0 a_{ic} \left(T_{ic}^j - T_{sa} \right) \tag{14.25}$$

$a_{ic} = \pi / 4 \, d_{eq}^2 L$ is the heat transfer area of the inner casing cell on the annulus side. d_{eq} is the equivalent diameter of the outer surface of the inner casing and L is its length. α_0 is the heat transfer coefficient of Eq. 8.13.

14.6.2 Calculation of Inner Casing Temperatures

The temperatures through the inner casing are of no great consequence to any of the thermodynamic processes taking place in the turbine. However, two situations of interest can be identified for which a more precise calculation of inner casing temperatures will be needed. Both are related to turbine supervisory measurements. The first is the expansion of the inner casing and, derived from it, the differential between turbine shaft and inner casing expansions and the monitoring of

gland seal clearances. The second is the estimation of rotor temperatures used for rotor stress calculations. Since rotor stresses cannot be directly measured, at least given the present state of technology, they must be estimated. Some turbine monitoring systems use the measured casing temperatures as proxy for the adjacent shaft surface temperature as the starting point for estimation of rotor temperatures and stress margins.

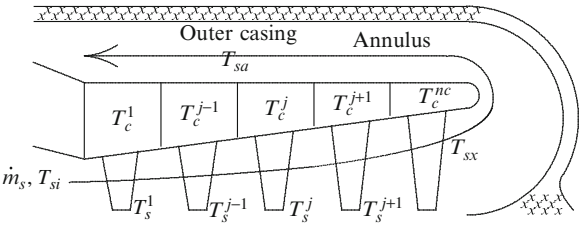

The notation can be made more compact by defining

$$\bar{\alpha}_{bl,j} = (\alpha_{bl}\, a_{bl}\, n_{bl})^j \quad \text{and} \quad \bar{\alpha}_{ic,j} = (\alpha_{ic}\, a_{cas})^j .$$

A simple heat balance for each inner casing cell, including heat transfers on the blading ($\dot{q}_{bl}$) and annulus ($\dot{q}_{ic}$) sides and spatial discretisation of axial conduction along the casing, yields the following ordinary differential equation for the temperature of the j-th cell:

$$\begin{aligned}
(M_m c_m)\frac{\mathrm{d}T_{ic}^j}{\mathrm{d}t} &= \dot{q}_{bl}^j - \dot{q}_{ic}^{j-1} + \lambda\frac{A_x}{dl}\left(T_{ic}^{j-1} - 2T_{ic}^j + T_{ic}^{j+1}\right) \\
&= \bar{\alpha}_{bl,j}\left(T_s^j - T_{ic}^j\right) - \bar{\alpha}_{ic,j}\left(T_{ic}^j - T_{sa}\right) \\
&\quad + \lambda\frac{A_x}{dL}\left(T_{ic}^{j-1} - T_{ic}^j + T_{ic}^{j+1}\right) \\
&= -\left(\bar{\alpha}_{bl,j} + \bar{\alpha}_{ic,j} + 2\lambda\frac{A_x}{dL}\right)T_{ic}^j + \lambda\frac{A_x}{dL}\left(T_{ic}^{j-1} + T_{ic}^{j+1}\right) \\
&\quad + \bar{\alpha}_{bl,j}\, T_s^j + \bar{\alpha}_{ic,j}\, T_{sa},
\end{aligned} \tag{14.26}$$

where M_m and c_m are the mass and material specific heat capacity of the casing metal in the cell. dL is the length of a casing cell, assumed equal for all cells.

Under normal on-load flow conditions, the steam transit time through the annulus is very short, and the steam temperature within the annulus T_{sa} will be indistinguishable from the turbine exhaust temperature T_{sx}. Even under conditions of very low or zero flow, such as during initial warming or during cooldown after a turbine trip, these temperatures are unlikely to be noticeably different. However, the calculation of the outer casing temperature is facilitated if we treat the annulus

temperature as distinct from the temperature of the steam at the turbine blading exhaust.

Setting

$$\varpi = \bar{\alpha}_{bl,j} + \bar{\alpha}_{ic,j} + 2\lambda \frac{A_x}{dL} \quad \text{and} \quad \tau = \frac{M_m c_m}{\varpi}$$

this equation can be rewritten

$$\tau \frac{\mathrm{d}T_{ic}{}^{j}}{\mathrm{d}t} + T_{ic}^{j} = \frac{\lambda\, A_x}{dL}\left(T_{ic}^{j-1} + T_{ic}^{j+1}\right)/\varpi + \left(\bar{\alpha}_{bl,j}\, T_s^j + \bar{\alpha}_{ic,j}\, T_{sx}\right)/\varpi. \quad (14.27)$$

Taking j over all n_c inner casing cells, Eq. 14.27 creates a system of n_c differential equations for the inner casing cell temperatures, given the appropriate boundary temperatures and steam flow.

Given the presence of terms for temperature in the (j-1)th and (j+1)th cells in Eq. 14.27, an obvious approach to its solution would be the replacement of the time derivative by its discrete time equivalent and reorganisation of the equation into a tridiagonal form incorporating the boundary temperatures at each end of the casing. However, given that the casing temperatures vary more slowly than the surrounding steam temperatures, the individual equations may be solved sequentially. Using the boundary condition defined for $j = 0$, the procedure starts from $j = 1$ and moves through all cells to $j = n_c$, using the just calculated value of T_{ic}^{j-1} and the previously calculated value of T_{ic}^{j+1}. The calculation for the final cell will use the boundary temperature defined for $j = n_c+1$.

As Leyzerovich points out [62], there is little theoretical basis for choosing a reliable heat transfer coefficient formula for the casing and field data must be relied on, ultimately. However, in the absence of such data, reasonable estimates can be provided by the conventional formula and adjusted to fit a given turbine. Leyzerovich presents a selection of field data which can assist.

14.6.3 Outer Casing Temperature

The outer casing of an HP turbine is relatively thick and well insulated. It is heated by convective transfer from the steam and to a much lesser extent by conduction from connecting parts, such as gland seals and bearings. Since conduction is relatively small compared with convective heat transfer under most circumstances, it will be represented in a very much simplified form, chosen more to facilitate the representation of cooldown than warm-up, for which it is of less importance.

The interest in the outer casing stems primarily from the need to calculate the differential expansion between the casing and the turbine shaft. Turbine supervisory measurements use this to monitor outer casing gland seal clearances. Of secondary but still significant importance is the reproduction of the cooldown behaviour of the turbine.

As mentioned previously, a simplified approach is sufficient for calculation of the annulus conditions. With h_{sa} the representative enthalpy of the steam within the annulus and c_{sa} its nominal heat capacity, a simple heat balance on the steam within the annulus produces

$$c_{sa}\frac{h_{sa}}{dt} = \dot{m}_{sx}(h_{sx} - h_{sa}) + \sum_j \dot{q}_{ic,j} - \dot{q}_{oc}, \tag{14.28}$$

where the heat transfer $\dot{q}_{ic,j}$ from the steam within the j-th zone of the turbine blading is given by Eq. 14.25. If we assume that the outer casing can be represented sufficiently well by a single temperature T_{oc}, heat transfer to the outer cylinder $\dot{q}_{oc}$ is

$$\dot{q}_{oc} = \alpha_{oc} A_{oc}(T_{sa} - T_{oc}), \tag{14.29}$$

where A_{oc} is the area in contact with steam. α_{oc} is the heat transfer coefficient at the inner surface of the outer cylinder and will be adequately approximated by the standard Hausen form. The annulus steam temperature follows from

$$T_{sa} = T(h_{sa}, p_{sa}).$$

The casing temperature follows from

$$(cm)_{oc}\frac{\mathrm{d}T_{oc}}{\mathrm{d}t} = \dot{q}_{oc} - \dot{q}_{amb} - \mathcal{C}_{cool}(T_{oc} - T_{ref}), \tag{14.30}$$

where the heat loss through the outer cylinder to ambient is

$$\dot{q}_{amb} = \bar{\alpha}_{insul}(T_{oc} - T_{amb})$$

T_{ref} is some temperature towards which the casing will cool in the long term. It may be a bearing temperature or ambient. Given the complex geometries of turbine components, the precise identification of the various possible conduction paths is extremely complex and need not be attempted. Instead, the coefficient $\mathcal{C}_{cool}$ can be chosen to match the known or expected long-term cooldown rate of the casing as in practice this will be the principal behaviour of interest.

A further comment of Leyzerovich [62] is of interest. As regards the long-term cooldown behaviour of the turbine, convective heat exchange by steam within the turbine chambers is considered to play no role in defining the cooldown transients, these being dominated by axial conduction from the shaft and casings to the end seals and bearings.

14.6.4 Heat Transfer to the Moving Blades

The main interest in heat transfer to the moving blades is the calculation of the turbine shaft temperatures and the derived thermal stresses since most heat

transferred to the turbine shaft passes through the moving blades. The greater emphasis in the literature is given to gas turbines for which the problem of blade temperatures is much more acute and greater attention must be paid to maximum blade temperatures and cooling requirements. Where relevant it has been assumed that the conclusions developed for gas turbine blading will apply equally to steam turbine blading with the substitution of steam parameters and properties.

With the turbine rotating, steam will flow axially along the turbine shaft, with minimal radial component outwards along the blade face. At any point the velocity of the steam relative to the blade surface is the rotational velocity of the blade $w = r\omega$, where r is the radial distance [m] of the steam from the shaft centre line and ω is the rotational speed of the shaft in radians/s. The Stanton number St is defined as

$$St = \frac{\alpha_1 v}{c_p w},$$

where α_1 is the heat transfer coefficient at the blade surface [kW/(m^{2}K)], v is the steam specific volume and c_p is the steam specific heat [kJ/(kg K)]. We then have the heat transfer coefficient from

$$\alpha_1 = \frac{c_p w St}{v}. \tag{14.31}$$

The Stanton number can be obtained from the Prandtl number P_r and Fanning friction factor ξ via the following relationship:

$$St = \frac{\xi/2}{1 + f(P_r)\sqrt{\xi/2}}. \tag{14.32}$$

By fitting to Fig. 8.4.23, p. 426 of Traupel, Vol. I [61], the function $f(P_r)$ is approximated by

$$f(P_r) = -8.0194 + 8.3791 P_r - 0.3597 P_r^2. \tag{14.33}$$

The Prandtl number for steam moves in the range from 5.8 at 20°C to around 0.9 at 600°C. It has a second-order dependency on pressure which can be ignored with little error. The following table summarises the values of P_r for steam for the indicated range of pressure and temperature (Perry [17], Table 3-304, p. 3-242).

At a pressure of 20 bar, the Prandtl number may be approximated from this table by

$$P_r = 1.616 - 0.2506\left(\frac{\mathcal{T}}{100}\right) + 0.02177\left(\frac{\mathcal{T}}{100}\right)^2 \tag{14.34}$$

to within 1%.

We may assume that the turbine blades are hydraulically smooth and that a reasonable constant for ξ will be in the range 0.035–0.05 at normal steam flows, increasing to around 0.1 at low steam flows (low Reynolds numbers $< 60{,}000$,

Bar	Temperature (K)								
	300	350	400	450	500	600	700	800	900
1	5.81	2.32	0.980	0.967	0.955	0.936	0.920	0.906	0.891
5	5.82	2.32	1.340	0.983	0.973	0.947	0.925	0.907	0.892
10	5.82	2.32	1.340	0.983	1.028	0.947	0.925	0.907	0.892
20	5.80	2.32	1.340	0.979	1.190	0.999	0.946	0.912	0.893
40	5.78	2.31	1.340	0.977	0.862	1.080	0.975	0.924	0.895
60	5.74	2.31	1.340	0.976	0.859	1.190	1.008	0.934	0.899
80	5.72	2.31	1.340	0.975	0.856	1.330	1.046	0.946	0.902
100	5.69	2.31	1.340	0.975	0.853	1.740	1.088	0.960	0.905
150	5.64	2.30	1.340	0.974	0.842	–	1.220	0.994	0.916
200	5.59	2.29	1.340	0.974	0.833	–	1.380	1.014	0.925

typical of start-up warming). Given the unpredictable complexities of flows under start-up conditions, these values are to be treated with some caution. Reasonable deviations found when fitting to actual plant data should not cause any surprises.

14.7 Turbine Shaft Metal Temperatures

The allowable rate of warming of a turbine shaft is the most significant parameter in defining the maximum start-up rate of the steam turbine. The primary objective of the start procedure is to minimise the start-up time while remaining within the allowable shaft temperature stress limits. These are related directly to the gradient of temperature in the radial direction. Most modern turbines, and all large turbines, are equipped with some form of shaft stress monitoring and limitation system. Since shaft temperatures are not measured, these systems require estimation of the profile of temperatures at selected points through the shaft. High-pressure valve chests and turbine casings and flanges may also be subject to stress monitoring and limitation. For these, actual temperature measurements are provided by thermocouples embedded at key locations within the component.

14.7.1 Calculation of the Temperature Field

For simulation purposes, a spatial field of time-varying metal temperatures in shafts and casings will be required:

1. As estimates of temperatures to be used for stress calculations by monitoring systems
2. For the calculation of shaft and casing expansion and differential expansion measurements

The calculation of metal temperature fields is greatly complicated by the irregular shapes and boundaries of the components. For design purposes, this usually

Fig. 14.5 A view of an LP turbine showing the steam flow path (courtesy of Millmerran Operating Company, Australia)

necessitates the use of finite element analysis with a large number of elements generating a fine mesh field. For operational simulation purposes, the accuracy requirements can be relaxed, permitting the assumption of more regular shapes and a smaller number of individual elements or cells.

Temperatures within a cylindrical shaft are defined by the unsteady heat conduction equation, Eq. 10.2 of Chap. 10.

$$\frac{1}{r}\frac{\partial T}{\partial r} + \frac{\partial^2 T}{\partial r^2} + \frac{\partial^2 T}{\partial z^2} = \frac{1}{D}\frac{\partial T}{\partial t}.$$

Boundary condition temperatures are related to the interfacing systems by specific instances of the generic Eqs. 10.38 and 10.39 for the radial (r) ordinate and Eqs. 10.40 and 10.41 for the axial (z) ordinate. The solution follows from application of the *alternating direction implicit* or ADI method, discussed in Sect. 10.2.

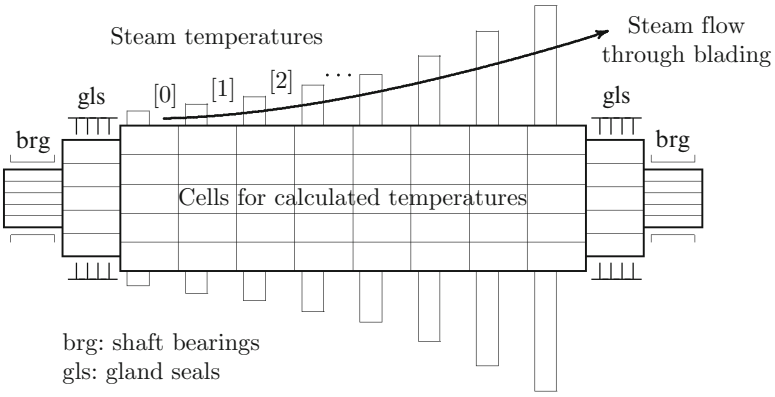

Consider a cylindrical shaft of the following geometry.

The central section of the shaft carries the blade rows. Each row consists of a number n_{bl} of individual identical blades set into the shaft and defines a cylindrical disk normal to the axis of rotation. This disk is treated as defining a single axial zone of length dL where $dL = L_{sb}/n_{rows}$ and n_{rows} is the number of blade rows distributed over the length of the blade zone L_{sb}. The reference or boundary temperature for the j-th axial zone is the local steam temperature Ts_j in contact with the blades. Of the generic boundary condition equations at the surface of an axial zone, Eqs. 10.38 and 10.39, only one need be applied for heat transfer at the outer surface of the shaft.

$$T_{-1} = T_1 - \frac{2\alpha_j \Delta r}{\lambda}(T_0 - Ts_j). \tag{14.35}$$

Recall that the earlier discussion of the ADI method applied to a hollow cylinder with heat transfer across both inner and outer surfaces. For the turbine shaft, we use symmetry to calculate the temperature distribution through half the shaft ($r_i < r < r_o$) and assume that the radial gradient of temperature along the centre line is zero, that is, $\partial T/\partial r = 0$ for $r = 0$. As mentioned in Chap. 10, we artificially assume a small $r_i > 0$, as if the shaft has a small bore hollow centre, which in reality it may indeed have, and the inner surface boundary condition is then more correctly $\partial T/\partial r = 0$ for $r = r_i$.

The heat transfer coefficient at the blade interface is given by Eq. 14.31. Two zones are provided at each end of the shaft linking the shaft to the gland sealing steam and to the shaft bearings. These provide the radial boundary conditions for the respective zones. It is apparent that the bearing lubricating oil must absorb heat conducted along the hot shaft. This will add to and usually exceed by a large margin the heat generated within the oil film in the journal bearings. These bearings usually operate at a higher temperature than others, in excess of 80°C, and require a suitable high temperature lubricating oil.

Most turbines are equipped with a thrust bearing to prevent lateral displacement of the shaft. This is commonly a Babbitt-type tilting pad bearing located between the HP and IP cylinders.

Temperatures at the axial ends of the shaft are set by the interfacing systems. All turbines will connect at one end of the shaft, sometimes at both, to some form of driven device, usually a pump, fan, blower (something between a fan and compressor) or compressor. In multi-cylinder turbines used for power generation, the shaft will either continue to the next section of blading or will be joined by a flanged connection to the shaft of the next cylinder. Between cylinders, the shaft will pass through gland seals and be supported by one or more bearings. In each case, the driving end boundary temperature will be taken from the connecting shaft. The external temperature at the non-driving end can be treated as ambient, with an appropriate heat transfer coefficient interposed between the shaft metal and the surrounding ambient.

In the radial direction the shaft is treated as a series of concentric cylindrical zones centred about the shaft centre line. Since symmetrical heating can usually be assumed[2], the spacing of the individual zones can be equal for all. The number of zones is selected to give a balance between computation load and accuracy.

14.8 Turbine Supervisory Measurements

Turbine supervisory instrumentation or TSI is widely used for the supervision, control and condition monitoring of all sizes of turbines, both steam and gas. In many applications, TSI is a mandatory requirement. It encompasses a range of measurements including vibrations, thermal expansion of shaft and casings, shaft eccentricity, rotor axial position, thrust bearing movement and rotor speed. Its purpose is to enhance the reliability of the turbine by supervising the operating parameters of the machine, identifying departures from normal which may indicate incipient damage and provide the quantitative basis for sound operational decisions, both automated responses and manual intervention by operating personnel.

14.8.1 Vibrations

Vibrations have been discussed in Sect. 7.5.3 within the context of bearings. It is true that most vibration measurements on rotating machines are taken from bearing housings as these provide the closest access to the shaft and the earlier material applies here to turbines without change. Because of their size and complexity, being composite assemblies of multiple rotating elements, and in consideration of their significant economic asset and revenue values, vibration issues of large steam turbines deserve individual attention.

Vibrations are measured individually for each bearing. In modern turbines, three vibrations are measured or resolved—the equivalent or total vibration and its x- and y-components. Movement of the shaft within the bearing may also be measured, using differential proximity measurements. During operation, the shaft will precess within the bearing, and its path can be displayed on a polar plot of shaft position. This information can be valuable to the diagnosis of potential operating problems but is rarely used for on line operational guidance.

The representation of the vibration/shaft speed relationship for any bearing has been discussed in Sect. 7.5.3 and can be applied here without change.

[2] Some turbines may be accelerated during run-up using only a single throttle valve. This can induce asymmetric flow through the blading and uneven heating.

14.8.2 Shaft Eccentricity

This is a measure of the degree of bending of the shaft. After an extended outage a turbine shaft, being of considerable length and mass suspended between two points (bearings), will bend downwards under its own weight, the point of maximum deflection being located about the mid-point of the axial separation of the suspension points. This will cause the ends of the shaft in the bearings to deflect upwards (while the shaft is stationary) by a much smaller amount, from which deflection the central deflection can be calculated. The end-of-shaft deflection is measured as the *eccentricity*. Before the turbine can be restarted the eccentricity must be reduced to within an acceptable range. This is done by rotating the shaft slowly using the turning gear motor. Significant time may be needed to remove the shaft bend or bow before the turbine may be accelerated. A similar situation can arise following a trip of the turbine, in which case the bowing of the shaft is a result of sudden and uneven cooling. The situation mentioned earlier using a single valve for start-up can also produce increased eccentricity because of uneven heating of the shaft. This can be a problem for turbines using partial arc admission.

Eccentricity is measured by a proximity device at the hot end of the HP turbine shaft, as far from the casing as possible to minimise thermal influences. The measurement is effective only at low shaft speeds, such as turning gear speed, and in some designs is disabled above some preset speed. With the shaft turning at this low speed, eccentricity will slowly reduce and, once below its permissible threshold, this condition for speed raising will be satisfied. Failure of the eccentricity to reduce may indicate a permanent bow of the shaft, with expensive consequences.

Acceleration of a turbine with excessive eccentricity will result in high levels of vibration induced by the eccentric rotating force of the shaft. It is probable that a turbine attempting to start under this condition will be runback or shutdown by its protective systems.

14.8.3 Expansion and Differential Expansion

During start-up of the turbine, the shafts and casings of the individual cylinders are exposed to wide variations of steam temperatures and heat transfer conditions. These vary from cylinder to cylinder, with the HP and IP cylinders exposed to the largest variations and the LP cylinder(s) exposed least. In each cylinder, the rotor and casing(s) will warm towards the local steam temperature and expand. The reverse process—cooling—will occur during shutdown. Being of differing materials and exposed to differing steam conditions, rotors and casings will expand by differing amounts. In addition, while the shaft inside the casing may expand and contract without restriction, movement of the casing will be constrained by connected pipework. As the moving and stationary parts are separated by small clearances in places such as shaft seals and blade tips, care must be taken to avoid contact between

surfaces to avoid mechanical damage. The shaft is permitted little axial movement relative to its bearings, and the construction must ensure that bearings and shafts move together.

Thermal expansion of rotors and casings occurs in all three dimensions and to avoid excess stresses and distortions they must be free to move to accommodate these dimensional changes. The turbine is therefore not constructed as a solid unit but rather as a series of rigid components which can move freely with respect to each other, albeit in a carefully constrained fashion designed to preserve exact geometric alignments. Since rotation is not allowed, thermal movements are constrained to the axial and transverse directions. During initial commissioning some slight rotation is allowed to align the various sections of rotor axially but, once aligned, further rotation is prevented.

The term "differential expansion" is applied to the difference between shaft and casing expansions, as measured at a specific reference point associated with each casing, usually at the hot end of the casing. The rotating shaft is free to expand along its entire length and may therefore move differentially with respect to the casing at any point. The axial movement of a shaft is referred to some fixed or reference point, usually taken as the LP cylinder which moves relatively little. The LP cylinder may be fixed in relation to its associated condenser if water cooled or to a fixed foundation point if the condenser is air cooled and therefore not attached directly to the turbine cylinder. If there are multiple cylinders, each is referred to its own datum.

It is normal practice to measure the actual position of the thrust bearing. As previously mentioned, this is usually located on its own pedestal, together with a bearing, between the HP and IP cylinders. A fixed reference is established, called the *key phasor*, which serves as a reference position for the thrust bearing. This bearing's position is taken as an indication of the balance of axial forces imposed by the axial steam flow on the shaft.

Expansion is expressed as a positive length, being the expansion of the component from its state at the reference temperature for which expansion is zero. Differential expansion can be positive or negative.

Each bearing is supported on a concrete pedestal which supports both bearings and casings. In some designs, HP and IP and/or IP and LP shafts may share a common bearing in which case both casings will be supported on the same pedestal, together with the bearing. Bearings and casings are free to slide axially, and casings laterally, along sliding keys embedded in the pedestal support structure. Saying that the casings move freely is optimistic. A casing or bearing imposes a considerable weight on its sliding support. With time, the sliding interface can become contaminated, and significant stiction can develop. Thermally induced movement of the casing may then not be smooth but can exhibit sudden steps as the expansion force increases beyond the stiction force and is relaxed by a sharp movement.

As the range of temperatures experienced by the LP cylinder, perhaps 160°C or so, is much less than that seen by either the HP or IP cylinders—in the range of 540–600°C—thermal expansion of the LP cylinder(s) is of less operational concern.

However, the expansion and differential expansion of all cylinders will normally be monitored.

The expansion of any component can be calculated simply from

$$e_{xp} = \beta \Delta T \, L, \tag{14.36}$$

where e_{xp} is the expansion, β is the material's coefficient of linear thermal expansion (K^{-1}) and L is the length of the component. e_{xp} will take the units of L. β is typically around 11.5e−6 K^{-1}. For a HP/IP shaft with a combined length of 15 m, a change of volumetric mean temperature of 350 K would produce an elongation of 63 mm over this length.

This is greatly in excess of observed data, a deviation due to the assumption that the entire shaft reaches this volumetric mean temperature. In reality only the heated part of the shaft, being that part of the shaft carrying the blades, might achieve this temperature, the remainder receiving no external heat and being comparable in length to the heated section. A more realistic calculation of shaft temperatures reduces this to around 45 mm. From a simulation perspective, these variations indicate the importance of reasonably accurate calculation of shaft and casing temperatures if parameters derived from them are to be realistic.

14.9 Shaft Stresses and Stress Evaluators

The simulation interest in turbine stress calculations stems from the need to drive the turbine's shaft and valve chest monitoring and limitations systems. These are commonly known as wall (WSE), rotor (RSE) or turbine (TSE) stress evaluators. Individual turbine manufacturers have proprietary systems which use black-box models of thick-walled and shaft components to estimate temperature profiles within the component and from these to estimate thermal stresses. By comparing estimated stresses to material limits, the system can determine allowable operating margins. Should any margin reduce below a preset limit, a warning is issued to operating staff and some form of active intervention may be initiated by the automation system. This will usually take the form of the blocking of further shaft speed or turbine load increase but may initiate a reduction in either of these, as appropriate to the plant's operating phase. The material limit values are selected to protect the component against plastic deformation or surface embrittlement (which can lead to surface cracking) or, as is now often the case, to minimise loss of material fatigue life.

The fields of elasticity, stress analysis and their influence on mechanical design are large and mature. It is well beyond the scope of this book to cover any of these fields to any depth. We will therefore confine discussion to a summary of the most fundamental principles and of the operational considerations which motivate this interest.

The turbine shaft is exposed at all times to deforming stresses. These are induced by centrifugal forces imposed by the shaft's rotation and by thermal expansion and contraction induced by heat transfer from and to the steam or gas. Bending forces on the blades are imposed at the root by centrifugal force and as reaction forces to the pressure of steam on the blades. The shaft itself may be subject to strong compressive forces imposed by blade rings which are heat-shrunk onto the shaft. Moreover, the complex shape of the shaft and blade connection arrangements create local regions of stress concentration.

During the design stage detailed stress analyses are conducted, usually using FEA techniques and exact shaft and blade profiles. These methods serve to define expected and minimum stresses in the rotor but are much too complex and time-consuming for online use. They are replaced for operational stress monitoring by very much simplified stress estimators based on simplified geometries, measurements of actual steam and casing metal temperatures and estimates of shaft metal temperatures.

Somewhere between these two sits simulation, where everything is calculated. Computer performance limitations dictate the use of simplified models for the calculation of shaft stresses and for the calculation of the casing, shaft and blade metal temperature fields upon which the stress calculations are based.

We will consider stresses arising from centrifugal and thermal effects only. We will assume that the turbine shaft (and blades where appropriate) can be represented by simple shapes. The turbine shaft is treated as a uniform extended cylinder, solid or bored, of radius r_o and the blades as a point mass located at a rotational radius r_e from the axis of rotation. The stress on the blade root is notionally located at the outer surface of the rotor cylinder.

For the shaft, thermal and centrifugal shaft stresses are calculated for each of the three cylindrical coordinates, tangential, radial and axial. Only the radial centrifugal stress is considered for the blades.

By way of introduction we will briefly summarise the fundamental concepts of elasticity.

14.9.1 Fundamental Concepts

When subject to a deforming force (tensile or compressive), any solid material will change its shape in each dimension by an amount related to the value of the deforming force. If the deformation returns to zero after removal of the deforming force, that is, the material regains its original shape, the deformation is said to have been elastic. If some deformation remains after removal of the deforming force, the deformation is said to be plastic and the material has exceeded its elastic limit. The stress to which the material is subjected is the component of the deforming force in the selected coordinate direction divided by the area of the material normal to the force and has the dimension of pressure. For a force which remains below the

material's elastic limit, the ratio of the applied stress, denoted σ, to the resulting *relative* deformation[3] called strain and denoted ϵ, is a constant. This is summarised by Hooke's law.

$$\frac{\sigma}{\epsilon} = E, \tag{14.37}$$

where E is the Young's Modulus of the material.

Application of a force to a slab of material in, say, the z direction (Cartesian coordinates) will cause a deformation in the z direction. This will be an elongation for a tensile force and a reduction for a compressive force. At the same time and in response to the same force, most materials will deform in each of the other directions but in the opposite sense. An elongation in the z direction will be accompanied by a reduction in both the x and y directions. The measure of the degree to which this occurs is the Poisson's ratio, denoted ν. It is the negative ratio of the transverse strain ϵ_x to the axial (in the direction of the force) strain ϵ_z.

$$\nu = -\frac{\epsilon_x}{\epsilon_z} \tag{14.38}$$

and is constrained to the range $(0, 0.5)$.

In the general case it is necessary to consider the stresses developed in each of the three coordinate directions. These are the principal stresses and, in Cartesian coordinates, are denoted σ_x, σ_y and σ_z. In cylindrical coordinates, they are the radial stress σ_r, the tangential or azimuthal stress σ_θ and the axial stress σ_z. Generalised to three coordinates, Hooke's law becomes

Cartesian Coordinates

$$\begin{aligned}
\epsilon_x &= \frac{1}{E}\left(\sigma_x - \nu(\sigma_y + \sigma_z)\right), \\
\epsilon_y &= \frac{1}{E}\left(\sigma_y - \nu(\sigma_x + \sigma_z)\right), \\
\epsilon_z &= \frac{1}{E}\left(\sigma_z - \nu(\sigma_x + \sigma_y)\right).
\end{aligned}$$

Cylindrical Coordinates

$$\begin{aligned}
\epsilon_r &= \frac{1}{E}\left(\sigma_r - \nu(\sigma_\theta + \sigma_z)\right), \\
\epsilon_\theta &= \frac{1}{E}\left(\sigma_\theta - \nu(\sigma_r + \sigma_z)\right), \\
\epsilon_z &= \frac{1}{E}\left(\sigma_z - \nu(\sigma_r + \sigma_\theta)\right).
\end{aligned}$$

[3] If an element of length L changes length by ΔL, $\epsilon = \Delta L / L$.

Assuming the material to be isotropic, both E and ν are the same in all directions.

Thermal expansion can be included in each of these strain expressions by the addition of the term $\beta\Delta T$, where β is the coefficient of thermal expansion of the material and ΔT is the differential between the local temperature of the material and some reference temperature for which the thermal expansion can be taken to be zero. In many cases, this will be taken as the volumetric mean temperature of the material. Then, in cylindrical coordinates, the individual strain terms, including thermal expansion, become

$$\epsilon_r = \frac{1}{E}(\sigma_r - \nu(\sigma_\theta + \sigma_z)) + \beta\,\Delta T,$$
$$\epsilon_\theta = \frac{1}{E}(\sigma_\theta - \nu(\sigma_r + \sigma_z)) + \beta\,\Delta T,$$
$$\epsilon_z = \frac{1}{E}(\sigma_z - \nu(\sigma_r + \sigma_\theta)) + \beta\,\Delta T.$$

For a body subjected to multidimensional deforming forces, the approach towards a stress limit can be difficult to predict on the basis of principal stresses, taken individually. It is therefore useful to define a composite stress factor which includes contributions from the individual stresses. The equivalent volumetric stress σ_{eq} due to von Mises (1923) can be used for this purpose. This is calculated as

$$\sigma_{eq} = \frac{1}{\sqrt{2}}\sqrt{(\sigma_1 - \sigma_2)^2 + (\sigma_2 - \sigma_3)^2 + (\sigma_3 - \sigma_1)^2}. \tag{14.39}$$

Being a scalar σ_{eq} can be easily compared to a reference value and used to indicate an approaching limit. As formulated by von Mises, it was hypothesised that a material would reach its yield point should the stress σ_{eq} reach some critical value, known as the von Mises yield strength. In what follows here σ_{eq} will be calculated from operational conditions and compared to a known limit value, which may itself depend on operating conditions, to initiate an appropriate automated intervention.

Within a significant band centred on the normal operating range of a turbine shaft, the shaft and casing materials remain within their elastic limits. We may therefore assume that the materials remain isotropic and that stresses arising from differing causes may be summated linearly to give composite results.

14.9.2 Centrifugal and Thermal Stresses in a Solid Cylindrical Shaft

This subject is covered comprehensively in Traupel [61] Vol. 2. With some reorganisation of the results quoted there, we may write the following equations

for the centrifugal radial $\sigma_{r\omega}$, tangential $\sigma_{\theta\omega}$ and axial $\sigma_{z\omega}$ stresses at any radius r measured from the axis of rotation.

$$\sigma_{r\omega} = \frac{3-2\nu}{8(1-\nu)}\rho\,\omega^2(r_o^2 - r^2), \tag{14.40}$$

$$\sigma_{\theta\omega} = \frac{3-2\nu}{8(1-\nu)}\rho\,\omega^2 r_o^2 - \frac{1+2\nu}{8(1-\nu)}\rho\,\omega^2 r^2, \tag{14.41}$$

$$\sigma_{z\omega} = \frac{\nu(3-2\nu)}{4(1-\nu)}\rho\,\omega^2 r_o^2 - \frac{\nu}{2(1-\nu)}\rho\,\omega^2 r^2 \tag{14.42}$$

ω is the speed of angular rotation of the shaft in radians/second. ρ is the density of the shaft material[4], and β is the coefficient of linear expansion.[5] The Poisson's ratio ν can be taken as 0.3 for steels used in turbine construction.

Traupel derives expressions for the thermal stresses in each of the cylindrical coordinates. For the radial and tangential stresses in a solid cylinder, we have

$$\sigma_{rT} = \frac{E\beta}{1-\nu}\int_r^{r_o}\frac{1}{r^3}\left(\int_0^r r^2\frac{\mathrm{d}T}{\mathrm{d}r}\mathrm{d}r\right)\mathrm{d}r, \tag{14.43}$$

$$\sigma'_{rT} = \frac{E\beta}{1-\nu}\frac{1}{r^3}\int_0^r r^2\frac{\mathrm{d}T}{\mathrm{d}r}\mathrm{d}r, \tag{14.44}$$

$$\sigma_{\theta T} = r\sigma'_{rT} + \sigma_{rT}. \tag{14.45}$$

The equations for σ_{rT} and σ'_{rT} can be expanded as follows, using integration by parts. Recall that integration by parts follows the rule

$$\int v\frac{\mathrm{d}u}{\mathrm{d}r}\mathrm{d}r = uv - \int u\frac{\mathrm{d}v}{\mathrm{d}r}\mathrm{d}r.$$

To expand the integral

$$I = \int_r^{r_o}\frac{1}{r^3}\left(\int_o^r r^2\frac{\mathrm{d}T}{\mathrm{d}r}\mathrm{d}r\right)\mathrm{d}r$$

set

$$I = \int_r^{r_o}\frac{1}{r^3}I_1\mathrm{d}r \text{ with } I_1 = \int_o^r r^2\frac{\mathrm{d}T}{\mathrm{d}r}\mathrm{d}r.$$

[4] usually steel, around 7,800 kg/m^3.

[5] typically around 11.5e−6 per K.

To integrate by parts, set

$$u = T; \quad v = r^2 \longrightarrow \frac{\mathrm{d}v}{\mathrm{d}r} = 2r; \quad u\frac{\mathrm{d}v}{\mathrm{d}r} = 2rT; \quad uv = Tr^2.$$

Then

$$I_1 = \left[Tr^2 - \int 2Tr\,\mathrm{d}r\right]_0^r = Tr^2 - 2\int_0^r Tr\,\mathrm{d}r.$$

Therefore,

$$I = \int_r^{r_o} T\frac{1}{r}\mathrm{d}r - 2\int_r^{r_o} \frac{1}{r^3}\left(\int_0^r Tr\,\mathrm{d}r\right)\mathrm{d}r.$$

Consider next the integral

$$I_2 = \int_r^{r_o} \frac{1}{r^3}\left(\int_0^r Tr\,\mathrm{d}r\right)\mathrm{d}r.$$

Again, integrating by parts, set

$$\frac{\mathrm{d}u}{\mathrm{d}r} = \frac{1}{r^3} \longrightarrow u = -\frac{1}{2r^2}; \quad v = \int_0^r Tr\,\mathrm{d}r \longrightarrow \frac{\mathrm{d}v}{\mathrm{d}r} = Tr.$$

Then

$$\begin{aligned} I_2 &= \left[-\frac{1}{2}\frac{1}{r^2}\int_0^r Tr\,\mathrm{d}r + \frac{1}{2}\int T\frac{1}{r}\mathrm{d}r\right]_r^{r_o} \\ &= -\frac{1}{2}\frac{1}{r_o^2}\int_0^{r_o} Tr\,\mathrm{d}r + \frac{1}{2}\frac{1}{r^2}\int_0^r Tr\,\mathrm{d}r + \frac{1}{2}\int_r^{r_o} T\frac{1}{r}\mathrm{d}r. \end{aligned}$$

Therefore,

$$\begin{aligned} I &= \int_r^{r_o} T\frac{1}{r}\mathrm{d}r + \frac{1}{r_o^2}\int_0^{r_o} Tr\,\mathrm{d}r - \frac{1}{r^2}\int_0^r Tr\,\mathrm{d}r - \int_r^{r_o} T\frac{1}{r}\mathrm{d}r \\ &= \frac{1}{r_o^2}\int_0^{r_o} Tr\,\mathrm{d}r - \frac{1}{r^2}\int_0^r Tr\,\mathrm{d}r. \end{aligned}$$

Define

$$\vartheta_m = \frac{2}{r_o^2}\int_0^{r_o} Tr\,\mathrm{d}r$$

to be the volumetric mean shaft temperature. The radial stress then becomes

$$\sigma_{rT} = \frac{E\beta}{1-\nu}\left[\frac{1}{2}\vartheta_m - \frac{1}{r^2}\int_0^r Tr\,\mathrm{d}r\right]. \tag{14.46}$$

The second bracketed term can be interpreted as half the volumetric mean temperature of that volume of the shaft between the centre line and the radius r.

The equation for σ'_{rT} can be expanded into

$$\sigma'_{rT} = -\frac{E\beta}{1-\nu}\frac{1}{r^2}\left[Tr^2 - 2\int_0^r Tr\,\mathrm{d}r\right]$$

giving for $\sigma_{\theta T} = r\sigma'_{rT} + \sigma_{rT}$

$$\sigma_{\theta T} = \frac{E\beta}{1-\nu}\left[\frac{1}{2}\vartheta_m + \frac{1}{r^2}\int_0^r Tr\,\mathrm{d}r - T\right]. \tag{14.47}$$

Finally the axial stress σ_{zT} may be written, from

$$\begin{aligned}\sigma_{zT} &= \nu(\sigma_{rT} - \sigma_{\theta T}) - E\beta\,\Delta T\\ &= \frac{\nu}{1-\nu}(\vartheta_m - T(r)) - E\beta\,\Delta T.\end{aligned}$$

The temperature differential ΔT is the difference between the local temperature $T(r)$ and a reference temperature. Setting the reference temperature to the volumetric mean temperature ϑ_m allows us to reduce this equation to

$$\sigma_{zT} = \frac{E\beta}{1-\nu}(\vartheta_m - T(r)). \tag{14.48}$$

Once a temperature field within the shaft has been determined using, for example, the analysis method of Sect. 14.7, the respective mean volumetric temperatures can be determined from numerical integration and the stresses calculated for any radial position.

During warming of the shaft the outer zone is subject to thermal compressive forces and the inner zone to thermal tensile forces. During cooling this situation is reversed. The centrifugal force is always tensile and is greatest at the shaft centre, reducing to zero at the surface. However, the blades add a radial centrifugal tensile stress normal to the rotor surface plane.

The accuracy of the stresses calculated using Eqs. 14.46–14.48 for a cylindrical shaft will ultimately depend on the accuracy of the metal temperatures used for their calculation. Even the proprietary TSE systems must be "calibrated" against design calculations, and a similar approach can be taken here by the provision of calibration constants to allow for both matching to expected stress values and to compensate for the effects of possibly coarse temperature cell quantization. And of course, the fairly gross simplifications introduced by the assumed geometry of shaft and blading will have a significant and adverse influence on overall accuracy.

Fig. 14.6 A view of LP turbine blading and its attachment (courtesy of Millmerran Operating Company, Australia)

14.9.3 Rotor Construction

The construction of the turbine rotor has considerable influence on the development of stresses in the shaft and blade disks. Individual manufacturers prefer their own construction methods; HP, IP and LP rotors show differing characteristic methods and steam turbines differ significantly from gas turbines and axial flow compressors. It is not possible to provide a general stress calculation method which applies equally to all cases, but if attention is confined only to the actual shaft, that is, the rotating cylinder to which the blades are attached, the methods outlined in this section can be applied with reasonable expectations of success.

Construction of the turbine rotor, which includes the shaft and its attached blade rows, generally takes any of three principal forms. HP and IP steam turbines are frequently constructed as a solid cylindrical or near-cylindrical shaft into which the individual blades are set in grooves let into the cylinder surface. The blades are retained in the grooves by a variety of methods including lock-ways, bolts and welds. HP turbine blades are usually small and impose relatively small centrifugal forces. IP turbine blades are larger than those of HP turbines but still impose relatively small centrifugal forces. The principal HP and IP turbine stresses are thermal, and the shaft will sometimes be manufactured with a hollow bore to reduce thermal warming times. The centre bore might also be used for shaft warming.

The situation for LP turbines is very different, and other construction methods are used. While rotating at the same speed as the HP and IP shafts, unless in a cross-compound arrangement they rotate at half-speed, the LP blades are much longer (in excess of 1,100 mm in large machines), are more robust than those of the HP and IP turbines and impose much greater centrifugal and bending forces on their points of attachment. The LP blades are usually mounted into disks either slid onto the shaft

and located using a key-way and some form of locking device or are heat-shrunk onto the shaft. In some designs, the disks are integral with the shaft and the blades slide into key-ways set into the periphery. In all such cases, the shaft is of much smaller radius than the disks and the most significant stresses are centrifugal and bending at the foot of the blade rather than thermal. For this reason, operational stress monitoring is applied to the HP and IP turbines but not usually to the LP turbine, although some LP turbines are provided with thermal stress monitoring at the steam inlet.

The use of heat shrinking attachment imposes a compression force to the shaft in the plane of the disk. This exceeds the centrifugal force of the blades by a considerable margin. The compression force reduces with increasing shaft speed as the blade centrifugal force increases. However, the net force on the shaft remains compressive up to shaft speeds well in excess of the rated speed.

Gas turbines and axial flow compressors are frequently assembled as rows of disks retained by bolts, either a series of bolts at around half radius or a single central bolt. By reducing the mass of the rotor, this construction method reduces its thermal mass and is better suited to rapid speed and load changes. Some designs use welded disks in preference to a bolted assembly. The reader is referred to specialist texts such as [61, 62] for further details and drawings.

14.9.4 Rotor Stress Variations During a Cold Start

The variables of principal interest are the equivalent shaft stress σ_{eq}, the shaft volumetric mean temperature ϑ_m, the rotor surface temperature, being here the mean temperature of the outermost rotor radial zone, and the differential between this and the shaft mean volumetric temperature.

The maximum zonal temperature differential is that seen by the outermost radial zone which therefore experiences the greatest radial thermal stress and, as it happens, the greatest tangential thermal stress, both of these stresses being compressive. The outermost zone is subject to the blade centrifugal stress which, being tensile, counteracts the compressive thermal stress. As the rotor speed increases, the centrifugal stresses increase and heat transfer to the blades increases with the increasing heat transfer coefficient and steam temperature. The shaft (here, blade) surface temperature increases towards the steam temperature and at 3,000 rpm approaches it closely even at a relatively low steam flow rate.

Figures 14.7–14.10 show trends of various calculated variables for three different idealised cold start schemes. Each figure uses the following curve assignments and identifiers.

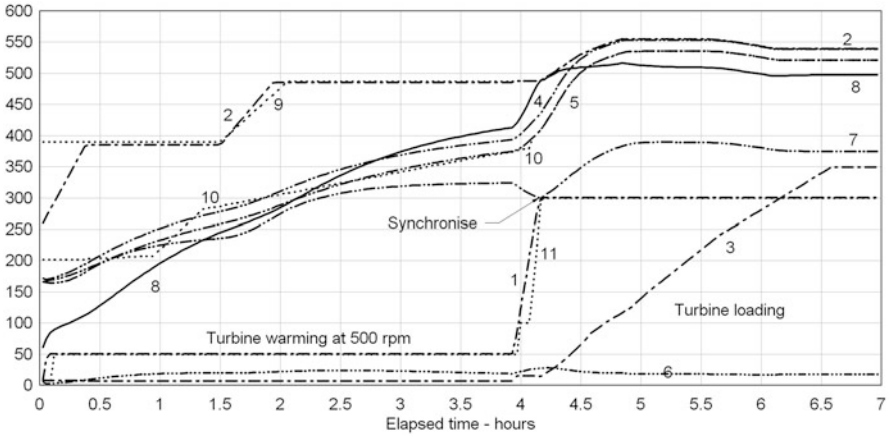

Fig. 14.7 Turbine cold start—warming at 500 rpm

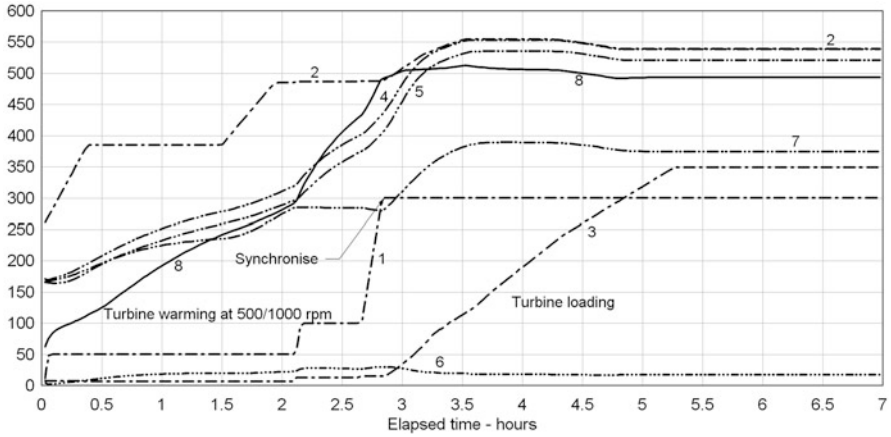

Fig. 14.8 Turbine cold start—warming at 500/1,000 rpm

1 — · — Turbine shaft speed [rpm/10]; 2 — · — Inlet steam temperature [°C];
3 — · — Steam flow to turbine [kg/s]; 4 — · ·— Shaft surface temperature [°C]
5 — · ·— Shaft average temperature [°C]; 6 — · · · — Shaft differential (sfc - avg) temperature [°C]; 7 — · ·— Turbine inner casing temperature [°C];
8 ——— Shaft equivalent stress σ_{eq} [MPa]

The first of these, Fig. 14.7, which we shall call the base case, shows results of a simulation matched to data available from a cold start of a 450 MW generating unit. The turbine model was set up with the design data of the HP cylinder. Steam and shaft temperatures were initialised to match as nearly as possible the plant's measured data, with the exception of main steam temperature which was allowed

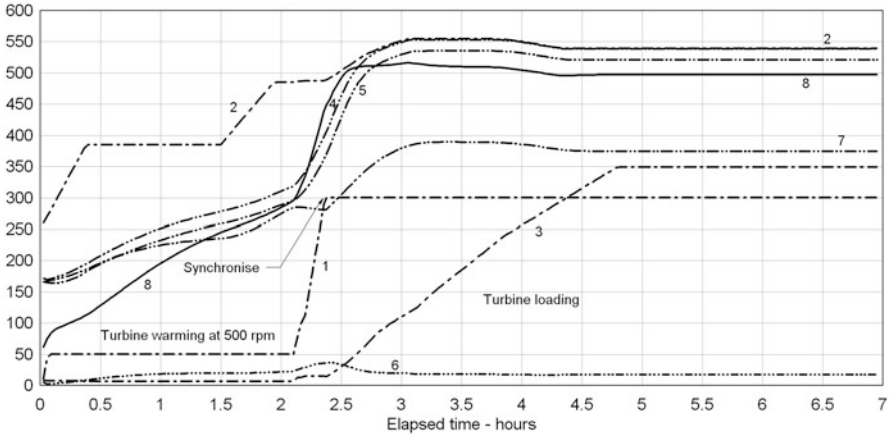

Fig. 14.9 Turbine cold start—warming at 500/1,000 rpm with early acceleration

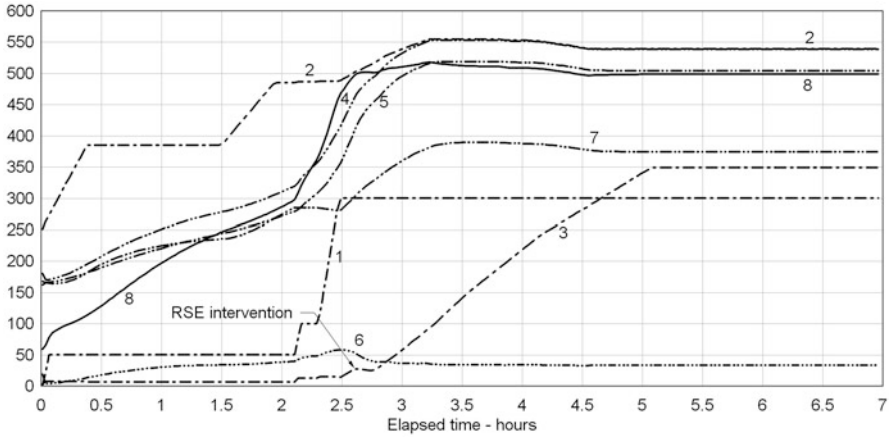

Fig. 14.10 Turbine cold start—early acceleration with RSE intervention

to increase at an operationally realistic rate from an initial 250°C to the measured 380°C. A lengthy period of pre-warming had established shaft surface, core and average temperatures at around 200°C, with the turbine rotated by the turning gear. The subsequent real plant time variations of turbine speed and steam temperatures were reproduced in the simulation by drivers.

The model behaviour was matched to that of the plant by adjustment of the turbine blade coefficient of heat transfer (Eq. 14.32) with the turbine rotating at 500 rpm. A value of 0.145 gave a good fit to the time taken to reach the real plant's shaft average temperature of 380°C, a value used during the cold start as release for shaft acceleration to 3,000 rpm for synchronising. Figure 14.7 includes selected plant data—shaft rotation speed (9, rpm/10), steam inlet temperature (10, °C) and

shaft average temperature (11, °C)—superimposed on the model calculated trends to allow comparison of the modelled and real plant values. No measured data has been included for the post-synchronisation phase as the real and simulated procedures differed in some detail. However, the general behaviour patterns were similar.

The "measured" shaft average temperature is of course not a physical measurement but a value calculated by a proprietary routine supplied by the turbine manufacturer as part of the rotor stress evaluator (the RSE, TSE or WSE mentioned earlier). The details of these calculations are not known to the simulation, and the various turbine "measurements"—shaft surface, core and average metal temperatures, as well as the stresses and margins calculated from them—must be generated by simulation-specific calculations such as those described here. Matching a simulation to a specific installation will require some knowledge of the RSE calculation method or, if this is unavailable, at least access to recordings of the RSE-calculated variables during a variety of unit starts.

Figures 14.8 and 14.9 show the same calculated trends for the same turbine but with differing speed profiles and acceleration criteria.

For Fig. 14.8, the turbine was held at 500 rpm for 2 h 10 min, then accelerated to 1,000 rpm and held at this speed until the shaft average temperature[6] exceeded the same threshold value of 380°C. This allowed the unit to be synchronised some 80 min earlier than the base case at no significant cost in the form of increased shaft stress or differential temperature increase. Figure 14.9 followed the same speed profile of Fig. 14.8 but allowed acceleration of the turbine once the shaft average temperature had exceeded the lower value of 310°C. The unit was synchronised some 100 min earlier than the base case but at the cost of increases in maximum stress and shaft differential temperature from 28°C for the base case to around 36°C.

To illustrate intervention by the RSE, most likely in the form of a hold on loading until the differential temperature returned below some lower threshold value, the method of calculation of the surface/shaft average temperature differential was changed slightly to cause it to increase above an expected limit of some 50°C. This situation is shown by Fig. 14.10, which repeats Fig. 14.9 with intervention triggered at >48°C and removed at <42°C. The action of the RSE delayed full load by around 20 min.

Although only a few of an infinite selection of possible start-up schedules, these examples serve to illustrate the process and suggest opportunities for start-up optimization.

[6] All of these temperatures and stresses are calculated for the inlet section, being the most highly stressed.